Applied Catalysis B: Environmental 88 (2009) 204–212

Contents lists available at ScienceDirect

Applied Catalysis B: Environmental

journal homepage: www.elsevier.com/locate/apcatb

Gold nanoparticles supported on manganese oxides for low-temperature CO oxidation

Lu-Cun Wang, Qian Liu, Xin-Song Huang, Yong-Mei Liu, Yong Cao *, Kang-Nian Fan

Department of Chemistry & Shanghai Key Laboratory of Molecular Catalysis and Innovative Materials, Fudan University, Shanghai 200433, PR China

ARTICLE INFO

Article history:
Received 6 August 2008
Received in revised form 10 September 2008
Accepted 29 September 2008
Available online 9 October 2008

Keywords:
Gold
Manganese oxide
Low-temperature oxidation of CO
Support effect

ABSTRACT

A series of gold catalysts deposited on various single-phase manganese oxides (MnO_x, including MnO_2, Mn_2O_3 and Mn_3O_4) were studied in relation to their performance in the low-temperature oxidation of CO. Gold was deposited onto the MnO_x support by deposition–precipitation with urea (DP urea). The activity of the Au/MnO_x catalysts for CO oxidation strongly depends on the nature of the manganese oxide support, ranking in the order $Au/Mn_2O_3 > Au/MnO_2 > Au/Mn_3O_4$. Transmission electron microscopy (TEM) results revealed different particle size distributions of gold for these Au-based catalysts, among which the Au/Mn_2O_3 catalyst showed the highest gold dispersion. Temperature programmed reduction (TPR) experiments indicated that the reducibilities of Au/MnO_x catalysts follow the same sequence with the activity. X-ray photoelectron spectroscopy (XPS) results suggested that both metallic and cationic gold species existed in the Au/Mn_2O_3 catalyst, while only metallic gold species were present in the other catalysts. The unique surface redox properties of Mn_2O_3 show great superiority for anchoring and dispersing of gold nanoparticles, which in turn leads to a higher reducibility of Mn_2O_3 and activity of the Au/Mn_2O_3 material for CO oxidation.

1. Introduction

Catalytic oxidation of CO has been of considerable interest recently due to its relevance in many industrial applications such as gas purification in CO_2 lasers, CO gas sensors, air-purification devices for respiratory protection, and pollution control devices for reducing industrial and environmental emission [1]. Conventionally, the use of noble metals such as Pt or Pd dispersed on various supporting materials for this reaction is well documented [2,3]. In recent years, supported gold catalysts have attracted tremendous attention owing to the notable discovery by Haruta that catalysts containing nanosized gold particles have extraordinary activities for low-temperature CO oxidation [4]. It has been well established that apart from the gold particle size, the choice of support plays a key role in the development of active gold catalysts [5–10]. Gold supported on reducible oxides is generally considered to be more active and stable than that supported on non-reducible oxides (SiO_2, Al_2O_3, etc.). Exceptionally high activities for CO oxidation have been reported for finely dispersed Au on reducible oxides, such as TiO_2, CeO_2, Fe_2O_3, Co_3O_4 and MnO_x [8–13]. The essential role of the reducible support is believed to provide oxygen adsorption and activation sites, possibly the oxygen vacancies or reactive perimeter sites at gold–oxide interface, which in turn can afford large amount of highly mobile oxygen species being able to react with CO [7,11].

Manganese oxides, both bulk and supported, have long been used as highly active, durable and low cost catalysts for various reactions such as the oxidation of carbon monoxide, methane and hydrocarbons [14–16]. When combined with gold nanoparticles, significantly enhanced activity has been achieved over Au/MnO_x system for CO oxidation [12,13,17–19] and solvent-free alcohol oxidation [20,21]. To date, the Au/MnO_x catalysts reported in the literature were mostly prepared by coprecipitation [12,13,18], which however has the disadvantage that the resulting gold particles are mainly embedded in an ill-defined manganese matrix comprising undecomposed Mn carbonates or multivalent manganese oxides. The complexity of the structural characteristics of the support along with the difficulty in controlling the Au particle size made it difficult to understand more deeply the catalytic mechanism of the Au/MnO_x catalysts [12]. It is thus of great interest to study the effects of support structure on the catalytic properties of Au/MnO_x catalysts by using phase-pure manganese oxides as the support materials.

In the present work, aiming to clarify the nature of the active sites and the role of the reducible oxide support in the catalytic behavior of gold catalysts, we investigated the catalytic activity of

* Corresponding author. Tel.: +86 21 55665287; fax: +86 21 65642978.
E-mail address: yongcao@fudan.edu.cn (Y. Cao).

0926-3373/$ – see front matter © 2008 Elsevier B.V. All rights reserved.
doi:10.1016/j.apcatb.2008.09.031

gold catalysts supported on single-phase manganese oxides with different phase structures, including MnO_2, Mn_2O_3 and Mn_3O_4, in the oxidation of CO. The structure–activity relationship of the Au/MnO_x materials are discussed in the light of a preliminary characterization of the physicochemical properties of the catalysts by X-ray diffraction (XRD), transmission electron microscopy (TEM), temperature programmed reduction (TPR) and X-ray photoelectron spectroscopy (XPS).

2. Experimental

2.1. Catalyst preparation

Three different kinds of manganese oxides nominal composition MnO_2, Mn_2O_3 and Mn_3O_4 were prepared using the solution-based or solid-state reaction procedures described in Refs. [22] as follows: (a) A 100 mL solution containing equal amount of $MnSO_4{\bullet}H_2O$ and $(NH_4)_2S_2O_8$ (both ca. 0.08 M) was hydrothermally processed at 393 K for 12 h followed by filtration and washing to obtain MnO_2. (b) Mn_2O_3 was prepared by calcination of $MnCO_3$ sample (AR) at 773 K in flowing air for 4 h. (c) Mn_3O_4 was obtained by an initial calcination of an $MnCO_3$ sample at 673 K in flowing N_2 for 4 h followed by an air exposure for 2 h.

Gold catalysts supported on the as-synthesized manganese oxides with a nominal Au loading of 8 wt.% were prepared by the method of deposition–precipitation with urea (DP Urea) as developed by Zanella et al. [23]. In a typical procedure, 3.6 g of urea was dissolved in 200 mL of 1.46 mmol L^{-1} $HAuCl_4$ solution with a nominal Au loading of 8 wt.% at room temperature. 1.86 g of MnO_2 support was then added to this solution. The temperature of the resulting slurry was increased gradually to 363 K and maintained for 4 h. The solid mass was filtered, washed several times with distilled water and dried at 373 K in air for 10 h. The Au/MnO_2 and Au/Mn_2O_3 samples were then calcined at 573 K for 4 h in static air. The Au/Mn_3O_4 sample was calcined at 573 K for 4 h in flowing N_2.

2.2. Catalyst characterization

The BET specific surface areas of the calcined catalysts were determined by adsorption–desorption of nitrogen at liquid nitrogen temperature, using a Micromeritics TriStar 3000 equipment. Sample degassing was carried out at 573 K prior to acquiring the adsorption isotherm. Elemental analysis with respect to Au loading was performed using ion-coupled plasma (ICP) atomic emission spectroscopy on a Thermo Electron IRIS Intrepid II XSP spectrometer. The samples were dissolved in a mixture of concentrated HCl and HNO_3 with volumetric ratio of 3/1 prior to the analysis.

TEM images were recorded on a JEOL 2011 electron microscope operating at 200 kV. Before being transferred into the TEM chamber, the samples dispersed with ethanol were deposited onto a carbon-coated copper grid and then quickly moved into the vacuum evaporator. The powder XRD patterns of the samples were collected on a Bruker D8 Advance X-ray diffractometer using nickel filtered Cu Kα radiation with a voltage and current of 40 kV and 20 mA, respectively.

TPR profiles were obtained on a homemade apparatus loaded with 20 mg of catalyst. TPR experiments were carried out in 5% H_2/Ar flowing at 40 mL min^{-1}, with a ramping rate of 10 K min^{-1} to a final temperature of 900 K. The H_2 consumption was monitored using a TCD detector. XPS spectra were recorded with a PerkinElmer PHI 5000C system equipped with a hemispherical electron energy analyzer. The Mg Kα ($h\nu$ = 1253.6 eV) was operated at 15 kV and 20 mA. The binding energy (BE) scale was referenced to the C 1s peak (284.6 eV) arising from adventitious carbon in the sample.

2.3. Catalytic activity tests

The catalytic activity tests were performed at atmospheric pressure in a quartz tube micro reactor (i.d. 3 mm). The catalyst weight was 50 mg, and the total flow rate of the reaction gas was 50 mL min^{-1}, with a composition of 1% CO–20% O_2 (balanced with He). Prior to CO oxidation reaction, the calcined gold catalysts were in situ treated under flowing He (20 mL min^{-1}) at 473 K for 0.5 h. The range of reaction temperature was from 200 to 673 K with a ramping rate of 2 K min^{-1}. The composition of the influent and effluent gas was detected with an online GC-17A gas chromatograph equipped with a TDX-01 column. The conversion of CO was calculated from the change in CO concentrations in the inlet and outlet gases. The turnover frequency (TOF) is calculated on the basis of surface gold atoms estimated by the model of hemispherical ball.

3. Results and discussion

3.1. Structural and textural properties of the catalysts

The physicochemical properties for various manganese oxides and corresponding Au/MnO_x catalysts are reported in Table 1. The measured BET data show that Mn_3O_4 has the highest BET surface area (59 m^2 g^{-1}) and the lowest one is observed for MnO_2 (10 m^2 g^{-1}). When gold was deposited onto the surface of the oxides, a moderately reduced BET surface area was identified for all Au-containing samples, with the variation trend unchanged. The specific surface areas are 10, 29, 46 m^2 g^{-1} for Au/MnO_2, Au/Mn_2O_3 and Au/Mn_3O_4 catalyst, respectively. The nominal gold loading is 3% for these catalysts. However, the real gold loading of these gold catalysts as determined by ICP-AES technique varied within the range of 2.2–2.9%. The diversity in gold loading level may be

Table 1
Physicochemical properties and catalytic activity results of various Au/MnO_x catalysts.

Sample	Au loading[a] (wt.%)	S_{BET} (m^2 g^{-1})	d_{Au}[b] (nm)	T_{max}[c] (K)	$T_{1/2}$[d] (K)	r_{CO}[e] ($mmol_{CO}$ g_{Au}^{-1} s^{-1})
MnO_2	–	16	–	642	427	–
Mn_2O_3	–	37	–	717	408	–
Mn_3O_4	–	59	–	732	503	–
Au/MnO_2	2.2	10	13.1	612	360	0.051
Au/Mn_2O_3	2.9	29	2.2	574	231	1.50
Au/Mn_3O_4	2.7	46	1.8/19.5[f]	730	411	0.014

[a] Determined by ICP-AES analysis.
[b] Average gold particle size estimated by statistical analysis from TEM results.
[c] The temperature at the maximum of the main reduction peak in the TPR profiles.
[d] The temperature at which the conversion was 50%.
[e] The specific reaction rate of CO oxidation at low conversions under a kinetically controlled regime at 298 K.
[f] The average size of the small gold particles and the average size of the large ones.

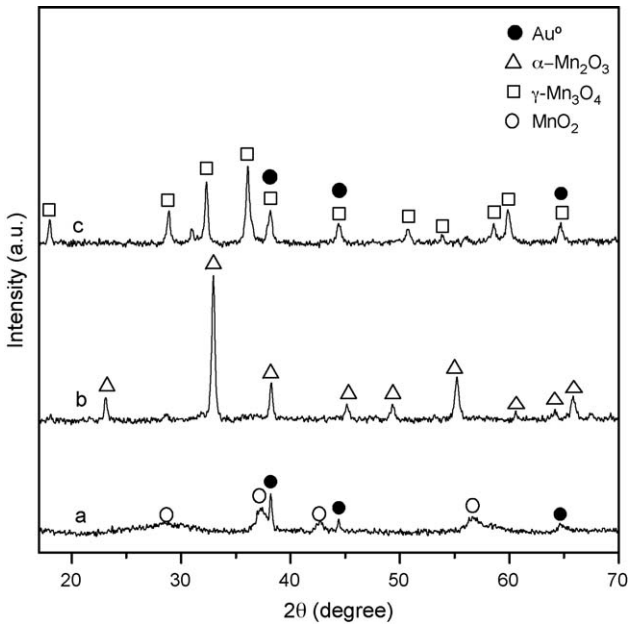

Fig. 1. XRD patterns of various MnO_x supported gold catalysts: (a) Au/MnO_2, (b) Au/Mn_2O_3 and (c) Au/Mn_3O_4.

related to the different surface acid–base properties of the manganese oxides originating from the various phase structures (as shown below).

Fig. 1 shows the XRD patterns of the as-prepared gold catalysts supported on different manganese oxides. It may be noted here that compared with the XRD patterns of the parent support materials (not shown here), the addition of Au produced no structural changes in the manganese oxide phases. The XRD pattern of the as-prepared Au/MnO_2 sample (Fig. 1a) is featured with broad and weak diffraction lines, which can be mainly attributed to a tetragonal phase of α-MnO_2 (JCPDS 44-0141). In addition, sharp diffraction peaks due to metallic gold crystallites can also be discerned, indicating the presence of large gold particles in the Au/MnO_2 sample. The XRD pattern of the as-synthesized Au/Mn_2O_3 sample (Fig. 1b) shows well-defined diffraction characteristics of α-Mn_2O_3 (bixbyite, JCPDS 41-1442). For the Au/Mn_3O_4 sample, all the reflections in the XRD pattern (Fig. 1c) could be perfectly indexed to γ-Mn_3O_4 (JCPDS 24-0734). No distinct gold reflections are visible in the patterns of samples Au/Mn_2O_3 and Au/Mn_3O_4, owing to the fact that the strongest reflection from gold overlaps with that of α-Mn_2O_3 and γ-Mn_3O_4 at $2\theta = 38.2^\circ$.

Representative transmission electron micrographs for the Au/MnO_2, Au/Mn_2O_3 and Au/Mn_3O_4 samples are shown in Fig. 2, where the metal particle size distribution established from the measurement of 200 particles with 95% confidence interval for each sample is also reported. The low-resolution electron micrograph shows that the MnO_2 is composed of small (10–30 nm) overlapping particles. Similar Mn_2O_3 particles were also observed with the Au/Mn_2O_3 catalyst, in sharp contrast to the distinct plate-like morphology of the Mn_3O_4 observed for the Au/Mn_3O_4 material. Easily detectable Au particles (evidenced by the arrow in Fig. 2) and a narrow distribution with an average particle size of ca. 2.2 nm have been observed in Au/Mn_2O_3. In contrast, the Au size distribution to Au/MnO_2 is broad indicating a large heterogeneity in size with a significant fraction larger than 10 nm. An even more interesting size distribution was identified for Au/Mn_3O_4. The catalyst displays a bimodal particle size distribution comprising two populations with average particle diameters of 1.8 and 19.5 nm, respectively. The mean gold particle size is 3.4 nm.

One notable advantage associated with the method of DP Urea for preparing supported Au catalyst is that complete deposition of gold onto TiO_2 or other oxide supports can be readily achieved [23], in contrast to the DP NaOH way in which much lower fraction of gold can be deposited [5]. However, the applicability of DP Urea still strongly depends on the nature of the substrate materials [24]. In this respect, it is not suitable for deposition of gold catalysts onto the oxide supports with point of zero charge (PZC) less than 6 [24]. In the present study, according to the literature [25–27], the PZC of MnO_2, Mn_2O_3 and Mn_3O_4 was determined to be <2.4, 6.7 and >10, respectively. Therefore, the presence of large gold particles and the relative lower gold loading for Au/MnO_2 sample can be well explained by the highly acidic nature of MnO_2. In contrast, small and uniform gold nanoparticles were obtained on the Mn_2O_3 thanks to its moderate PZC. As for Au/Mn_3O_4, the bimodal size distribution of gold particles may be caused by the inert pretreatment atmosphere. It has been reported that pretreatment of Au/TiO_2 catalyst in oxidic atmosphere can lead to the formation of positive gold species affording a stronger metal-support interaction and better stability against sintering [28]. In addition, a recent study on the nucleation of gold clusters on $TiO_2(1\,1\,0)$ surfaces in three different oxidation states showed that a much stronger Au oxide-support adhesion exists on O-rich Au-support interfaces than on O-poor oxide-support surfaces [29]. Likely, the treatment of Au/Mn_3O_4 sample in the inert atmosphere may lead to the reduction of AuO_x and the formation of oxygen-deficient Au-support interface bearing weak bonding strength, which may account for its poor stability against sintering. The bimodal size distribution of gold particles may be an indication for an Ostwald ripening mechanism [30], operating via detachment and condensation of mobile Au or AuO_x species.

3.2. Redox properties

TPR experiments were carried out to investigate the redox properties of various MnO_x-supported gold catalysts. Fig. 3 presents the reduction profiles of these catalysts. For comparison, the TPR profiles of the parent manganese oxides are also included. The temperatures at peak maximum (T_M) for various samples are given in Table 1. The MnO_2 sample exhibits two reduction peaks, the first one at 642 K ($7.55\,mmol_{H_2}\,g^{-1}$) and the second one at 723 K ($3.62\,mmol_{H_2}\,g^{-1}$), indicating the stepwise reduction of manganese oxides [31]. According to the literature, the low-temperature (LT) peak may be roughly attributed to the reduction of MnO_2 to Mn_3O_4, whereas the high-temperature (HT) peak is attributed to the consecutive reduction of Mn_3O_4 to MnO [31]. When Au was added to MnO_2, the two reduction peaks became closer and shifted to lower temperatures, with the ratio of H_2 consumption almost unchanged. This shift in the surface MnO_2 reduction with respect to Au addition can be attributed to the presence of spillover effect involving either hydrogen activated on the metal phase or the mobile lattice oxygen induced by intimate metal-support interactions [32].

The TPR profile of Au/Mn_2O_3 shows two peaks at temperatures above 470 K, with the highest T_M located at 574 K. A close comparison of the profile for Au/Mn_2O_3 with those for Mn_2O_3 and Au/MnO_2 catalysts reveals that the presence of Au nanoparticles strongly promotes Mn_2O_3 reduction, as reflected by the significant shift of the reduction maxima (T_M) of the main reduction peak to lower temperatures. Moreover, in contrast to the doublet reduction feature of Mn_2O_3 and Au/MnO_2 samples, the Au/Mn_2O_3 catalyst show additional low-temperature reduction feature of relatively

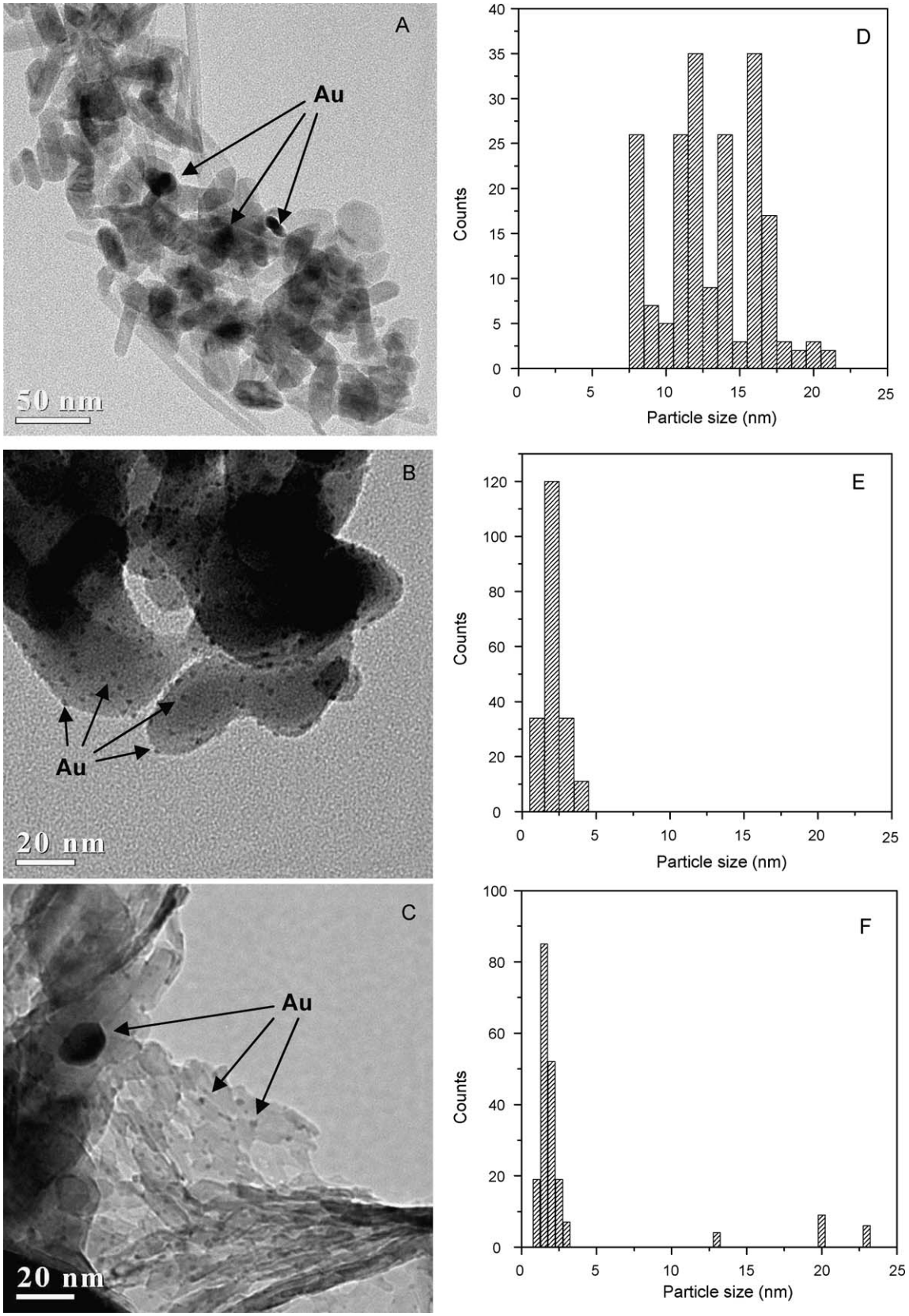

Fig. 2. TEM images and gold particle distributions of various MnO_x supported gold catalysts: (a) and (d), Au/MnO_2; (b) and (e), Au/Mn_2O_3; (c) and (f), Au/Mn_3O_4.

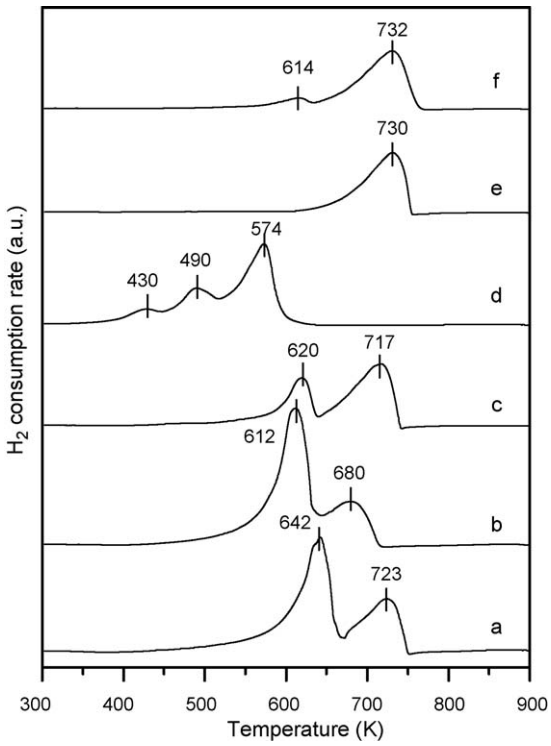

Fig. 3. TPR profiles of various MnO_x and corresponding supported gold catalysts: (a) MnO_2, (b) Au/MnO_2, (c) Mn_2O_3, (d) Au/Mn_2O_3, (e) Mn_3O_4 and (f) Au/Mn_3O_4.

weak intensity located at ca. 430 K (0.89 $mmol_{H_2}$ g^{-1}). This observation, together with the fact that the Au/α-Mn_2O_3 material shows comparable overall H_2 consumption (6.25 $mmol_{H_2}$ g^{-1}) with that for α-Mn_2O_3 sample (6.51 $mmol_{H_2}$ g^{-1}), strongly suggests that the manganese oxide substrates are "activated" to a larger extent in the Au/Mn_2O_3 catalyst.

For sample Mn_3O_4, the reduction profile contains only one peak at 730 K. The addition of gold resulted in the appearance of a new weak reduction peak at lower temperature (ca. 614 K, 0.75 $mmol_{H_2}$ g^{-1}), with the position of the main reduction peak (730 K, 3.06 $mmol_{H_2}$ g^{-1}) unaltered, indicating that the presence of gold has limited influence on the reducibility of Mn_3O_4 although the Au/Mn_3O_4 sample contains a proportion of small gold particles (Fig. 2f). At this juncture, it is interesting to point out that despite an appreciably larger average particle size, the reduction temperature of MnO_2 shifted to lower temperature when gold is added to MnO_2 support (see Fig. 3b). Presumably, the redox properties of the Au–Mn catalysts are largely determined by the specific nature of the Au-support interface rather than by the gold particle size.

3.3. Surface chemical states

The Au 4f XPS spectra of various Au/MnO_x catalysts before and after CO oxidation are presented in Fig. 4. Broad peaks of Au $4f_{7/2}$ and Au $4f_{5/2}$ states are observed in all Au/MnO_x samples, indicating the possible presence of both metallic and ionic gold species [33,34]. Fig. 4 illustrates the deconvolution analysis results of the Au 4f spectra for various catalysts. The detailed XPS parameters of all samples are summarized in Table 2. It was found that the Au 4f peaks with respect to Au/MnO_2 and Au/Mn_3O_4 samples before and after reaction could be well fitted by one component, suggesting that only one kind of Au species, i.e., Au^0, existed in the samples. In contrast, for sample Au/Mn_2O_3, quantitative deconvolution of the Au 4f peaks resulted in a composition of about 88% metallic (83.9 eV) and 12% partially oxidized Au species (86.2 eV) for the fresh catalyst. After CO oxidation reaction, the fraction of the oxidized Au species increased to 20% (Table 2), thus indicating the presence of two kinds of Au species in the Au/Mn_2O_3 catalyst. The

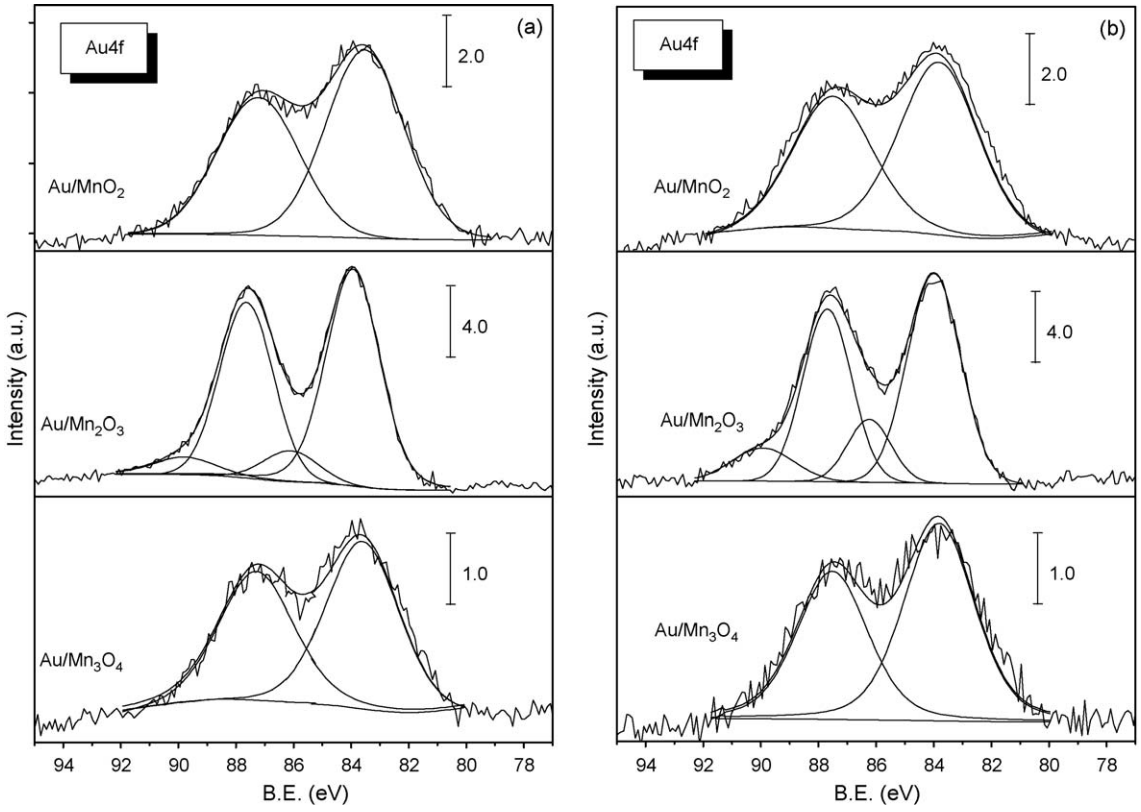

Fig. 4. Au 4f XPS spectra of various MnO_x supported gold catalysts before and after reaction: (a) fresh catalysts, (b) used catalysts.

Table 2
XPS results of Au/MnO_x catalysts before and after reaction in CO oxidation.

Catalyst	BE of Au $4f_{7/2}$ (eV)	Fraction of Au species (%)	BE of Mn $2p_{3/2}$ (eV)	Au/Mn	O_T/Mn[a]	O_L/Mn[b]
Au/MnO_2	83.8	100	642.0	0.026	2.39	1.24
Used Au/MnO_2	83.9	100	642.1	0.025	2.22	1.13
Au/Mn_2O_3	83.9	88	641.8	0.095	2.28	0.98
	86.2	12				
Used Au/Mn_2O_3	83.9	80	641.7	0.082	1.97	0.86
	86.2	20				
Au/Mn_3O_4	83.8	100	641.4	0.038	3.07	0.93
Used Au/Mn_3O_4	83.8	100	641.6	0.035	4.15	0.76

[a] O_T, total surface oxygen.
[b] O_L, surface lattice oxygen.

relative increase of the proportion of the positively charged gold species is understandable when considering the fact that excess oxygen is present under reaction conditions. Presumably, these cationic gold species are located at the Au-support interface. Similar to our findings, the presence of positively charged gold species has also been reported in the Au/CeO_2 system even after reductive pretreatment at 673 K [34]. By using Mössbauer spectroscopy in combination with a range of complementary spectroscopies, Daniells et al. [35] have proposed that cationic gold plays a crucial role in catalyzing CO oxidation over Au/Fe_2O_3 catalyst. In the present work, the absence of cationic gold species in the Au/MnO_2 and Au/Mn_3O_4 samples could be explained by the presence of large gold particles and the oxygen-poor nature of Au-support interface induced by the specific treatment conditions, respectively. It is known that large gold particles are difficult to oxidize under mild conditions. However, on considering the oxidative pretreatment of Au/MnO_2 catalyst, we cannot rule out the possibility that oxidized gold species are present at the perimeter between Au and MnO_2 with the amount being too low to be detected by XPS.

Fig. 5 compares the Mn 2p XPS spectra for various catalysts before and after reaction, respectively. The Au/MnO_2 catalyst shows an asymmetric Mn $2p_{3/2}$ peak located at 642.1 eV indicating the presence of Mn^{4+}. The BEs of Mn3/2 shifted to lower values in the following order: $Au/MnO_2 > Au/Mn_2O_3 > Au/Mn_3O_4$. In addition, it can be seen from Table 2 that there is no significant change in terms of BE for both fresh and spent catalysts. Additional information regarding the O 1s core level data of the Au/MnO_x materials is presented in Fig. 6. The O 1s main peak at ca. 529 eV is attributed to the lattice oxygen bonded to Mn atoms [13]. Moreover, distinct shoulders are visible on the high binding energy sides of the main peaks. Similar shoulder features have also been observed in the O 1 s XPS spectra of Au/MnO_x catalysts prepared by aqueous coprecipitation and were assigned to a mixture of hydroxyl groups and adsorbed water on the surface of catalysts [18]. As expected, the peak intensity with respect to lattice oxygen decreased following an order of $Au/MnO_2 > Au/Mn_2O_3 > Au/Mn_3O_4$. After reaction, the proportion of the oxygen species varied to different extents for these catalysts.

The surface compositions in terms of Au/Mn and O/Mn molar ratios are summarized in Table 2. It is clear that the Au/Mn_2O_3 catalyst has the highest Au/Mn ratio, which is an indication of the highest gold dispersion among the three catalysts. After reaction, no significant variation of the Au/Mn ratio was found for these catalysts except that of the Au/Mn_2O_3 catalyst, i.e., from 0.95 to 0.82. This may be caused by thermal sintering of the very small gold nanoparticles during the reaction. On the other hand, the molar ratios of the total amount of surface oxygen (O_T) to Mn are significantly higher than the stoichiometric value in the MnO_x materials. This indicates the presence of a high concentration of oxygen-containing adsorbates, most likely hydroxyl groups or water, on the surface of Au/MnO_x catalysts. The peak deconvolution of the O 1s lines gives more information about the relative amount of different surface oxygen species. As shown in Table 2, the molar ratios of surface lattice oxygen (O_L, 528. 7 eV) to Mn for all samples are smaller than the stoichiometric value in the corresponding MnO_x, inferring the presence of surface oxygen vacancies which however are filled by water or hydroxyl groups. It is believed that these oxygen vacancies could be regenerated under reaction conditions and could play a key role in the activation of adsorbed molecular O_2. After reaction, the O_L/Mn ratios decreased for all catalysts. This result may imply that the lattice oxygen of the Au/MnO_x catalysts participated in the oxidation reaction process.

3.4. Catalytic activity for CO oxidation

The catalytic performances of MnO_x-supported gold nanoparticles in CO oxidation are shown in Fig. 7, where the CO conversion is reported as a function of temperature (light-off test). For comparison, the activities of the parent manganese oxides are also included. It is clear that the activities of the supported gold catalysts are notably higher than those for the corresponding parent support materials, with the highest enhancement in activity being achieved over Au/Mn_2O_3 catalyst. The temperature at which the conversion was 50% ($T_{1/2}$) for Mn_2O_3 is 407 K, which is in good agreement with the literature results under similar conditions [36] and is 176 K higher than that for Au/Mn_2O_3 (Table 1). The $T_{1/2}$ value for the Au/MnO_2 catalyst was 360 K, ca. 70 K lower than the MnO_2 support. This is a little surprising when considering its relatively large gold particle size. In contrast, for the Au/Mn_3O_4 catalyst, despite the presence of very small gold particles (1–3 nm, see above), CO oxidation catalysis did not occur at low temperature as expected, since a 50% value of conversion is only attained well beyond 400 K. Furthermore, Table 1 compares the specific activities in terms of reaction rates (r_{CO}) that are normalized to gold mass for the three Au/MnO_x catalysts. It can be seen that the reaction rate follows the same trend with that in Fig. 7, i.e., $Au/Mn_2O_3 > Au/MnO_2 > Au/Mn_3O_4$. The reaction rate of the Au/Mn_2O_3 is almost two magnitudes higher than those of other two catalysts.

The catalytic activity of the Au/Mn_2O_3 catalyst was further compared with other reported gold catalysts in the oxidation of CO. The intrinsic activities in terms of the mass-specific reaction rates ($mmol_{CO}\ g_{Au}^{-1}\ s^{-1}$) based on total gold atoms as well as the turnover frequencies (TOF) based on surface gold atoms are listed in Table 3. It is known that the catalytic performance of gold catalysts can be greatly influenced by gold particle size, the type of support and reaction conditions [7]. Therefore, comparison of activities for different catalytic systems is usually difficult. However, there are general agreements that small gold particle size is indispensable for its high activity and that gold supported on reducible oxides is more active than gold supported on non-

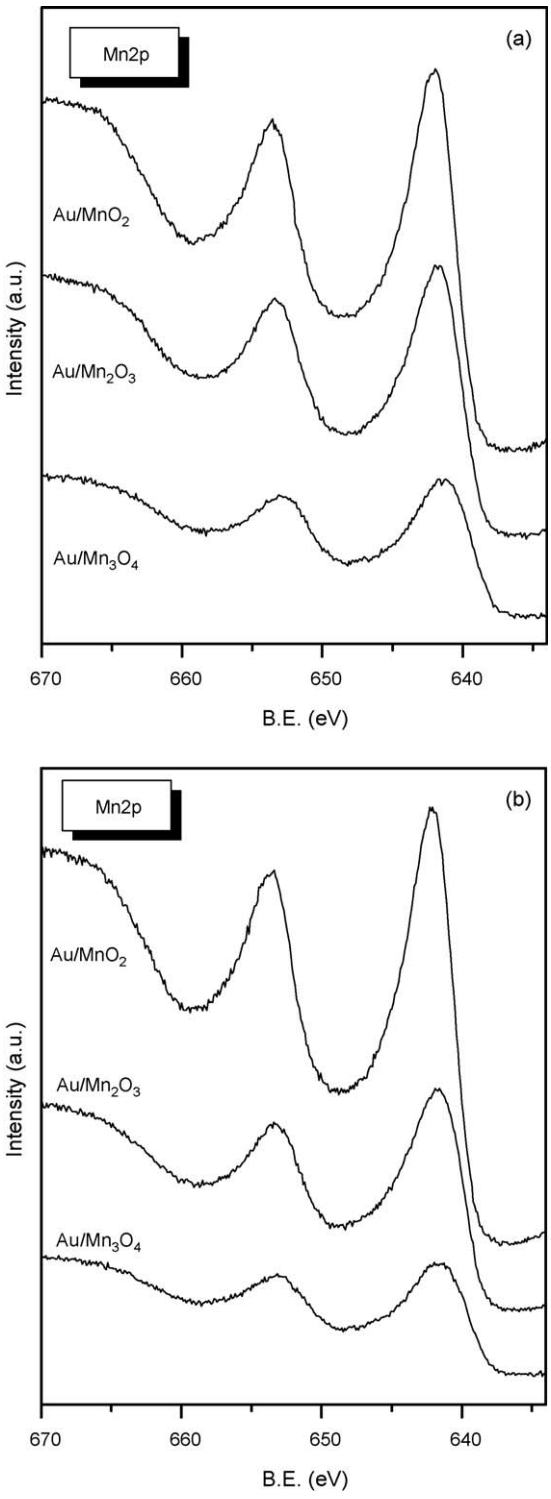

Fig. 5. Mn 2p XPS spectra of various MnO_x supported gold catalysts before and after reaction: (a) fresh catalysts, (b) used catalysts.

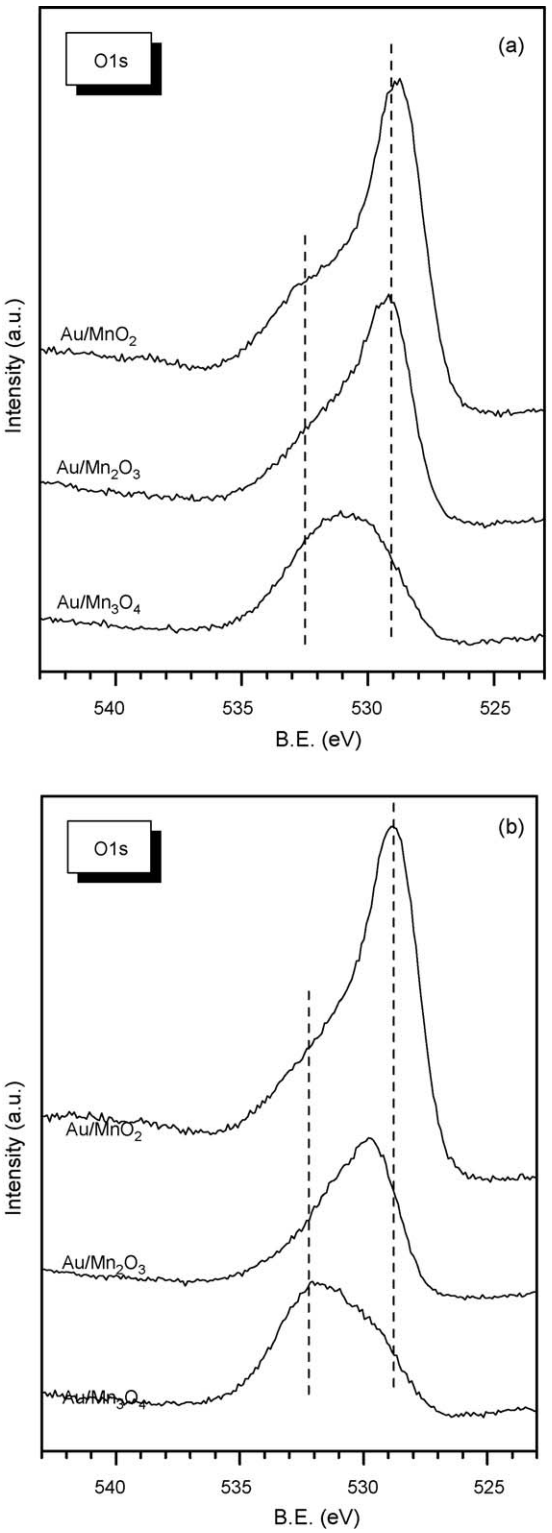

Fig. 6. O 1s XPS spectra of various MnO_x supported gold catalysts before and after reaction: (a) fresh catalysts, (b) used catalysts.

reducible oxides (e.g. SiO_2, γ-Al_2O_3) [5]. These conclusions can also be corroborated by the data presented in Table 3. A rough comparison of the mass-specific reaction rate and TOF with other gold catalysts under similar reaction conditions reveals that the Au/Mn_2O_3 catalyst appears to be among the most active Au-based catalysts reported thus far [8,37–40].

Based on the above activity results, it seems that the gold particle size is not the decisive factor to obtain a highly active gold catalyst in the low-temperature CO oxidation. While little or no clear correlation between catalytic activity and gold particle size has been identified in the literature, several other parameters such as the oxidation state of gold species and the metal-support interaction have been suggested as determining factors [7]. At this juncture, it is important to note that the present TPR experiments

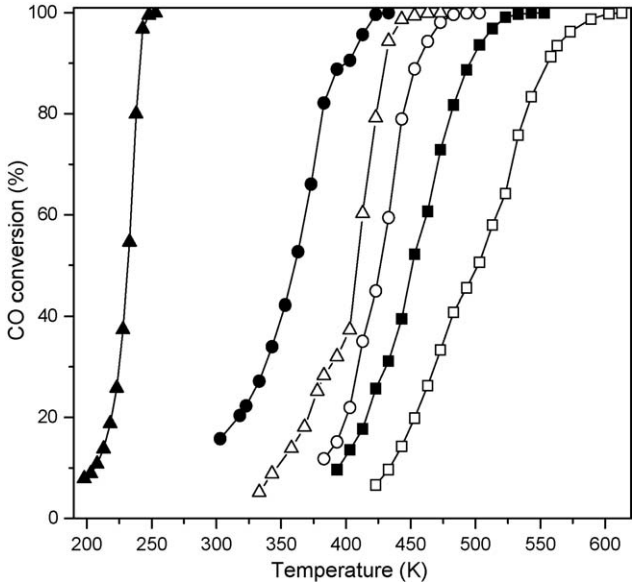

Fig. 7. The catalytic performance of various MnO_x and corresponding supported gold catalysts. (●) Au/MnO_2, (○) MnO_2, (■) Au/Mn_3O_4, (□) Mn_3O_4, (▲) Au/Mn_2O_3, (△) Mn_2O_3. Reaction conditions: 50 mg catalyst, 1% CO–20% O_2 balanced with He, 50 mL min^{-1}.

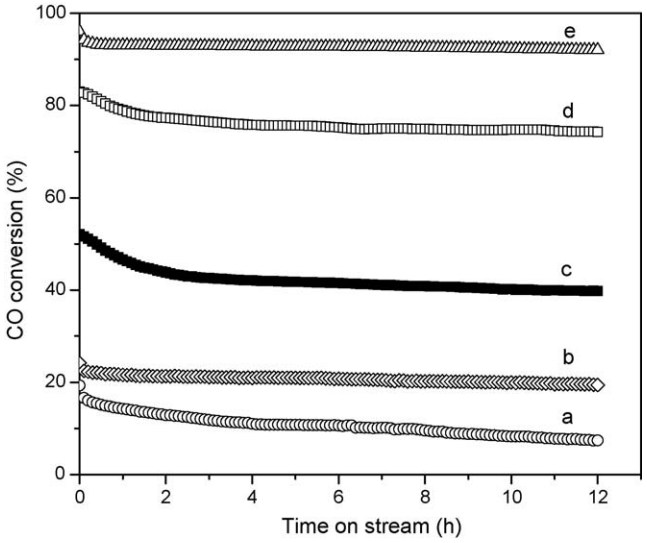

Fig. 8. Time-on-stream change of CO conversion over various MnO_x supported gold catalysts in a feed stream containing 1% CO and 20% O_2. (a) 200 mg Au/Mn_3O_4 at 323 K, (b) 50 mg Au/MnO_2 at 323 K, (c) 5 mg Au/Mn_2O_3 at 293 K, (d) 5 mg Au/Mn_2O_3 at 323 K, (e) 5 mg Au/Mn_2O_3 at 353 K.

clearly demonstrated that the reducibility of MnO_2 was improved to a larger extent by the addition of Au, as opposed to the Au/Mn_3O_4 system. This indicates the presence of a stronger metal-support interaction in Au/MnO_2 material, despite its slightly larger mean gold particle size. In this sense, it may be deduced that the metal-support interaction plays a more important role in controlling the activity of the catalyst. As for Au/Mn_2O_3, the highest activity can be well explained by the smallest mean gold particle size combined with its strongest metal-support interactions among these catalysts.

It has been widely accepted that CO oxidation over manganese oxides proceeds via the Mars-van-Krevelen mechanism which involves the reaction of adsorbed CO with the labile lattice oxygen [41]. The reactivity is associated with the capacity of manganese to form various oxidation states, e.g., redox reaction of Mn^{2+}/Mn^{3+} or Mn^{3+}/Mn^{4+}, and "oxygen mobility" in the oxide lattice. With respect to this, it is important to note that in the present study, the addition of gold can have notable influence on the redox properties of the manganese oxide supports. On the one hand, gold enhances the reactivity of manganese oxides by modifying the rate of vacancy exchange between the bulk and the oxide surface, and by facilitating the migration of oxygen vacancies from the bulk to the oxide surface [42]. On the other hand, the addition of Au can significantly promote the CO adsorption properties, consequently enhancing the reaction activity. Based on the above results, it is apparent that this promotional effect of Au was especially pronounced for the Au/Mn_2O_3 catalyst.

The catalytic stability of the various Au/MnO_x catalysts in CO oxidation at 323 K is compared in Fig. 8. To obtain reliable results of the stability, the mass of catalysts were adjusted to ensure that conversion was lower than 100%. In the experiments for all catalysts, a relatively strong initial deactivation was observed over the first 2 h after the catalyst was put on stream. The deactivation rate slowed down significantly in the period between 2 and 12 h on stream, slowly approaching a steady state. The most intensive deactivation occurred on the Au/Mn_3O_4 catalyst, with a loss of activity by 62% after 12 h on stream. The Au/Mn_2O_3 showed the best stability among the studied catalysts, with the activity decayed by 10% during the same period. It is worth mentioning that extended reaction time of 60 h at 323 K led to a further loss of activity by ca. 24%. Furthermore, the stability of the Au/Mn_2O_3 catalyst was tested at two different temperatures (293 and 353 K). It can be clearly seen that the relative decay was higher at lower reaction temperatures.

It has been suggested that two main factors may contribute to the deactivation of Au catalysts, i.e., the change of the morphology of gold nanoparticles induced by the exothermic nature of CO oxidation and the accumulation of carbonates blocking the active sites [43–45]. Considering the rather low activity of Au/Mn_3O_4 and Au/MnO_2 catalysts, it is unlikely that the deactivation is caused by the growth of gold particles. This speculation is further supported by

Table 3
Comparison of the specific activities for CO oxidation over various gold catalysts at 298 K.

Catalyst	d_{Au} (nm)	p_{CO}, p_{O2} (kPa)	r_{Au} ($mmol_{CO}\ g_{Au}^{-1}\ s^{-1}$)	TOF (s^{-1})	Refs.
Au/Mn_2O_3	2.2	1.0, 20	1.50	0.55[a]	This study
Au/Fe_2O_3	6.5	1.0, 20	0.36	0.30	[37]
Au/Fe_2O_3	3.6	1.0, air	0.18	0.086	[8]
Au/Co_3O_4	~2	1.0, air	0.44	0.48	[8]
Au/TiO_2	3	1.0, air	0.64	0.32	[8]
Au/TiO_2	2.9	1.0, air	0.64	0.26	[38]
Au/Al_2O_3	2.4	1.0, air	0.21	0.02	[39]
Au/SiO_2	6.6	1.0, air	0.05	0.02	[39]

[a] The turnover frequency (TOF) is calculated on the basis of surface gold atoms estimated by the model of hemispherical ball.

the XPS results of surface composition analysis, which indicate that the surface Au/Mn molar ratio experienced little change after reaction for the two catalysts (see Table 2). In contrast, the relatively larger change of Au/Mn ratio (from 0.95 to 0.82) over Au/Mn_2O_3 suggests that the growth of gold particles may partly account for its deactivation. This is particularly true when considering the strong exothermic effect associated with the high activity of Au/Mn_2O_3 catalyst. On the other hand, in line with previous spectroscopic observation [42], the improved stability of Au/Mn_2O_3 at higher reaction temperatures can be explained by an easier decomposition of surface-blocking carbonate species. This finding implies that the carbonate buildup during reaction may also play an important role in determining the stability of Au/Mn_2O_3.

4. Conclusion

Gold nanoparticles supported on various manganese oxides, including MnO_2, Mn_2O_3 and Mn_3O_4, have been prepared by DP urea method. The catalytic reactivity followed the order of $Au/Mn_2O_3 > Au/MnO_2 > Au/Mn_3O_4$ in the low-temperature oxidation of CO. TEM results revealed that very small gold nanoparticles were evenly dispersed on the surface of Mn_2O_3, while large gold crystallites were found on the other two support materials. TPR experiments indicated that the Au/Mn_2O_3 catalyst has the best redox properties among these catalysts, the trend of which coincided with that of the activity. XPS analysis suggested that both metallic and cationic gold species existed in the Au/Mn_2O_3 catalyst, while only metallic gold species were present in the other catalysts. We proposed that as compared with other Au/MnO_x catalysts, the superior performance of the Au/Mn_2O_3 catalytic system in low-temperature CO oxidation could be attributed to the presence of highly dispersed gold species and to the unique redox properties originating from the intimate metal-support interactions.

Acknowledgments

This work was supported by the National Natural Science Foundation of China (20421303, 20473021, 20633030, 20873026), the National Basic Research Program of China (Grant No. 2003CB615807), the National High Technology Research and Development Program of China (2006AA03Z336), the Committee of the Shanghai Education (06SG03) and the Committee of Shanghai Science and Technology (07QH14003).

References

[1] I. Dobrosz-Gómez 1, I. Kocemba, J.M. Rynkowski, Appl. Catal. B: Environ. 76 (2007) 107.
[2] D.S. Stark, A. Crocker, G.J. Steward, J. Phys. E: Sci. Instrum. 16 (1983) 158.
[3] D.S. Stark, M.R. Harris, J. Phys. E: Sci. Instrum. 16 (1983) 492.
[4] M. Haruta, T. Kobayashi, H. Sano, N. Yamada, Chem. Lett. 2 (1987) 405.
[5] G.C. Bond, D.T. Thompson, Catal. Rev. Sci. Eng. 41 (1999) 319.
[6] A.S.K. Hashmi, G.J. Hutchings, Angew. Chem. Int. Ed. 45 (2007) 7896.
[7] B.K. Min, C.M. Friend, Chem. Rev. 107 (2007) 2709.
[8] M. Haruta, S. Tsubota, T. Kobayashi, H. Kageyama, M.J. Genet, B. Delmon, J. Catal. 144 (1993) 175.
[9] K.Y. Ho, K.L. Yeung, Gold Bull. 40 (2007) 15.
[10] S. Carrettin, P. Concepción, A. Corma, J.M. Lopez Nieto, V.F. Puntes, Angew. Chem. Int. Ed. 43 (2004) 2538.
[11] M.M. Schubert, S. Hackenberg, A.C. van Veen, M. Muhler, V. Plzak, R.J. Behm, J. Catal. 197 (2001) 113.
[12] R.M.T. Sanchez, A. Ueda, K. Tanaka, M. Haruta, J. Catal. 168 (1997) 125.
[13] S.D. Gardner, G.B. Hoflund, M.R. Davidson, D.R. Schryer, J. Schryer, B.T. Upchurch, E.J. Kielin, Langmuir 7 (1991) 2135.
[14] G.G. Xia, Y.G. Yin, W.S. Willis, J.Y. Wang, S.L. Suib, J. Catal. 185 (1999) 91.
[15] K. Ramesh, L. Chen, F. Chen, Z. Zhong, J. Chin, H. Mook, Y.F. Han, Catal. Commun. 8 (2007) 1421.
[16] Y.F. Han, L. Chen, K. Ramesh, E. Widjaja, S. Chilukoti, I.K. Surjami, J. Chen., J. Catal. 253 (2008) 261.
[17] G.B. Hoflund, S.D. Gardner, D.R. Schryer, B.T. Upchurch, E.J. Kielin, Appl. Catal. B: Environ. 6 (1995) 117.
[18] S.J. Lee, A. Gavriilidis, Q.A. Pankhurst, A. Kyek, F.E. Wagner, P.C.L. Wong, K.L. Yeung, J. Catal. 200 (2001) 298.
[19] R.J.H. Grisel, B.E. Nieuwenhuys, Catal. Today 64 (2001) 69.
[20] L.C. Wang, Y.M. Liu, M. Chen, Y. Cao, H.Y. He, K.-N. Fan, J. Phys. Chem. C 112 (2008) 6981.
[21] L.C. Wang, L. He, Q. Liu, Y.M. Liu, M. Chen, Y. Cao, H.Y. He, K.-N. Fan, Appl. Catal. A: Gen. 344 (2008) 150.
[22] X.Q. Li, J. Xu, F. Wang, J. Gao, L.P. Zhou, G.Y. Yang, Catal. Lett. 108 (2006) 137.
[23] R. Zanella, S. Giorgio, C.R. Henry, C. Louis, J. Phys. Chem. B 106 (2002) 7634.
[24] R. Zanella, S. Giorgio, C.-H. Shin, C.R. Henry, C. Louis, J. Catal. 222 (2004) 357.
[25] M. Kosmulski, J. Colloid Interface Sci. 253 (2002) 77.
[26] M. Kosmulski, J. Colloid Interface Sci. 275 (2004) 214.
[27] M. Kosmulski, J. Colloid Interface Sci. 298 (2006) 730.
[28] K.Y. Ho, K.L. Yeung, J. Catal. 242 (2006) 131.
[29] D. Matthey, J.G. Wang, S. Wendt, J. Matthiesen, R. Schaub, E. Lægsgaard, B. Hammer, F. Besenbacher, Science 315 (2007) 1692.
[30] S. Kielbassa, A. Häbich, J. Schnaidt, J. Bansmann, F. Weigl, H.-G. Boyen, P. Ziemann, R.J. Behm, Langmuir 22 (2006) 7873.
[31] E.R. Stobbe, B.A. de Boer, J.W. Geus, Catal. Today 47 (1999) 161.
[32] H. Trevino, G.D. Lei, W.M.H. Sachtler, J. Catal. 154 (1995) 245.
[33] S.D. Gardner, G.B. Hoflund, M.R. Davidson, H.A. Laitinen, D.R. Schryer, B.T. Upchurch, Langmuir 7 (1991) 2140.
[34] R. Leppelt, B. Schumacher, V. Plzak, M. Kinne, R.J. Behm, J. Catal. 244 (2006) 137.
[35] S.T. Daniells, A.R. Overweg, M. Makkee, J.A. Moulijn, J. Catal. 230 (2005) 52.
[36] S. Imamura, Y. Tsuji, Y. Miyake, T. Ito, J. Catal. 151 (1995) 279.
[37] M.M. Schubert, V. Plzak, J. Garche, R.J. Behm, Catal. Lett. 76 (2001) 143.
[38] M.J. Kahlich, H.A. Gasteiger, R.J. Behm, J. Catal. 182 (1999) 430.
[39] G.R. Bamwenda, S. Tsubota, T. Nakamura, M. Haruta, Catal. Lett. 44 (1997) 83.
[40] M. Okumura, S. Nakamura, S. Tsubota, T. Nakamura, M. Azuma, M. Haruta, Catal. Lett. 51 (1998) 53.
[41] K. Ramesh, L. Chen, F. Chen, Y. Liu, Z. Wang, Y.-F. Han, Catal. Today 131 (2008) 477.
[42] J.A. Rodriguez, G. Liu, T. Jirsak, J. Hrbek, Z. Chang, J. Dvorak, A. Maiti, J. Am. Chem. Soc. 124 (2002) 5242.
[43] C.H. Kim, L.T. Thompson, J. Catal. 230 (2005) 66.
[44] Y. Denkwitz, Z. Zhao, U. Hörmann, U. Kaiser, V. Plzak, R.J. Behm, J. Catal. 251 (2007) 363.
[45] M. Azar, V. Caps, F. Morfin, J.-L. Rousset, A. Piednoir, J.-C. Bertolini, L. Piccolo, J. Catal. 239 (2006) 307.